

Proof of Concept: Local TX Real-Time Phase Calibration in MIMO Systems

Carl Collmann, Ahmad Nimir, Gerhard Fettweis

Vodafone Chair Mobile Communications Systems, Technische Universität Dresden, Germany

{carl.collmann, ahmad.nimir, gerhard.fettweis}@tu-dresden.de

Abstract—Channel measurements in multiple-input multiple-output (MIMO) systems hinge on precise synchronization. While methods for time and frequency synchronization are well established, maintaining real-time phase coherence remains an open requirement for many MIMO systems. Phase coherence in MIMO systems is crucial for beamforming in digital arrays and enables precise parameter estimates such as Angle-of-Arrival/Departure. This work presents and validates a simple local real-time phase calibration method for a digital array. We compare two different approaches, instantaneous and smoothed calibration, to determine the optimal interval between synchronization procedures. To quantitatively assess calibration performance, we use two metrics: the average beamforming power loss and the root mean square (RMS) cycle-to-cycle jitter. Our results indicate that both approaches for phase calibration are effective and yield RMS of jitter in the 2.1 ps to 124 fs range for different software-defined radio (SDR) models. This level of precision enables coherent transmission on commonly available SDR platforms, allowing investigation on advanced MIMO techniques and transmit beamforming in practical testbeds.

Index Terms—software-defined radio, multiple-input multiple-output, radio frequency transceiver

I. INTRODUCTION

Phase noise in multiple-input multiple-output (MIMO) communication systems significantly degrades data throughput [1] and in the context of joint communication and sensing (JCnS) limits the accuracy of parameter estimates [2]. The compensation of phase noise at the receiver side is well established. For example the 3GPP standard [3] offers the phase tracking reference signal (PT-RS) to compensate for the constant phase error (CPE) induced by phase noise. However to enable transmit beamforming in a digital array, coherence between radio frequency (RF) chains feeding the transmitting antenna array has to be assured.

There are several known calibration approaches in the literature, each with limitations. Reciprocity calibration Over-the-Air (OTA) with distributed sensor nodes such as [4] and [5] lacks a shared phase reference, making it unsuitable for coherent combination of the signals from multiple transmitters. In [6] a reciprocity calibration OTA scheme is employed where both transmit and receive arrays are connected to a common measurement device. This wired connection requires the transmitter and receiver to be co-located, making the approach unsuitable for mobile communication scenarios. The authors in [7] present OTA reciprocity calibration in MIMO systems, where all distributed radio units are connected to a central controller that performs synchronization by pre-coding

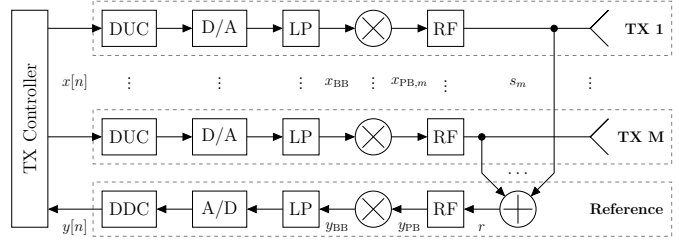


Fig. 1. Setup for phase calibration of TX array, comparison to reference.

with phase estimates. A limitation in this work is that the radio units have no method of compensating the local oscillator (LO) phase drifts internally, which imposes a significant overhead on the OTA calibration. Compounding these challenges, the often neglected residual transmit side calibration errors, can substantially degrade achievable MIMO throughput [8].

In this work, we address these limitations by proposing and validating a simple, local method for real-time phase calibration of transmit RF chains. Our approach uses a dedicated reference RF chain at the transmitter to receive calibration signals (PT-RS) from each transmit chain in a time-division multiple access (TDMA) scheme. The transmit-controller estimates the phase of each chain relative to this reference and applies precoding to achieve coherent transmission in passband. The calibration procedure is performed in periodic intervals to continuously track LO drift, to directly address the transmit side phase impairments as highlighted in [8].

The paper is organized as follows. Section II introduces the system model for local transmitter calibration and modeling of phase noise processes for voltage-controlled oscillator (VCO) and phase-locked loop (PLL). Section III presents measurement results and validates the calibration approaches. Section IV explores the effect of different calibration intervals and their impact on the achievable beamforming gain. Finally, the paper is concluded in section V with key results.

II. SYSTEM MODEL

A. Local Calibration of TX Array

Our objective is to calibrate the phase of each element in a transmitting digital antenna array with M elements, as illustrated in Fig. 1. To achieve this objective, the phases of the transmitting chains must be compared to a common reference. Because the transmitting chains and reference RF chain are co-

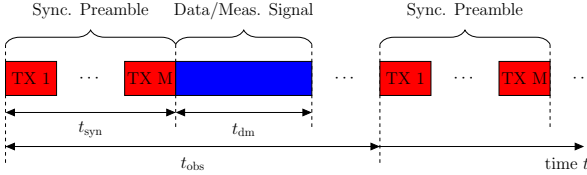


Fig. 2. Phase calibration scheme, periodic transmission of synchronization preamble, observed signal at transmitter reference.

located, we assume a common trigger signal (e.g., 1-pulse-per-second) to align the sampling clocks and a common 10 MHz reference are available. While the sampling clocks are considered as ideal, the synthesized carrier signals exhibit phase noise and corresponding drift. Further impairments considered are the phase responses of RF chain components and their respective RF front ends.

As shown in Fig. 2, each TX chain transmits a synchronization signal $x[n]$ of length N in TDMA before the data or measurement signal. The band-limited baseband signal after D/A conversion and low-pass filtering is denoted $x_{\text{BB}}(t)$, defined over $t \in [0, NT_s]$. After up-conversion, the bandpass signal for chain m becomes

$$x_{\text{BP},m}(t) = x_{\text{BB}}(t) e^{j(2\pi f_{c,m} t + \theta_{\text{OS},m}(t))}. \quad (1)$$

The synthesized carrier frequency $f_{c,m}$ is variable per chain to model a residual frequency offset. This small residual carrier frequency offset (CFO) models a linear phase shift over time, distinct from oscillator phase noise. The term $\theta_{\text{OS},m}(t)$ refers to the time-dependent phase of the oscillator signal for RF chain m . Then the transmitted signal at RF chain m in TDMA is

$$s_{\text{TX},m}(t) = x_{\text{BP},m}(t - mNT_s) e^{j\theta_{\text{RF},m}} \quad (2)$$

The term $\theta_{\text{RF},m}$ represents a constant phase shift specific to chain m . This shift arises from the cumulative phase response of amplifiers, switches, splitters, filters, and other front-end components. As illustrated in Fig. 2, the synchronization preamble has duration $t_{\text{syn}} = MNT_s$ and is repeated every t_{obs} seconds to obtain phase observations for each chain periodically. The locally received signal at the reference RF chain is the sum of the transmit signals

$$r_{\text{TX}}(t) = \sum_{m=1}^M s_{\text{TX},m}(t). \quad (3)$$

Down-converting using the reference chain's local oscillator at frequency f_c yields the baseband received signal

$$y_{\text{BB}}(t) = r_{\text{TX}}(t) e^{-j2\pi f_c t}. \quad (4)$$

Note that the received signal gain is neglected, assuming it is compensated by an automatic gain control (AGC). Furthermore, the phase shift of the RF components at the reference chain is neglected, as it will induce an identical phase shift for all $s_{\text{TX},m}(t)$ and only the relative phase relation of RF chains are of interest. For simplicity, the phase

noise introduced by the oscillator of the reference chain is neglected under the assumption that t_{syn} is sufficiently short. As a frequency offset are already modeled at the transmitting RF chain, the synthesized carrier frequency at the reference chain is assumed to be ideal.

Assuming $|x_{\text{BB}}(t)|^2 = 1$, the system function estimate for chain m is obtained by multiplying the received baseband signal with the complex conjugate of the transmitted signal and windowing to the appropriate TDMA slot:

$$\hat{h}_{\text{TX},m}(t) = y_{\text{BB}}(t) \cdot x_{\text{BB}}^*(t) \cdot \text{rect}\left[\frac{t - (m + \frac{N}{2}) T_s}{NT_s}\right]. \quad (5)$$

The time-dependent phase is then found as $\arg[\hat{h}_{\text{TX},m}(t)]$. Assuming this phase consists of a constant term with additive Gaussian noise, as elaborated on in section II-B, the optimal estimator is the time average [9]. Averaging this phase over the synchronization interval yields the phase estimate

$$\hat{\theta}_m = \frac{1}{NT_s} \int_0^{NT_s} \arg[\hat{h}_{\text{TX},m}(t)] dt. \quad (6)$$

The transmission controller Fig. 1 then uses these phase estimates to align all M transmitting RF chains. To achieve coherent transmission, the baseband data signal transmitted from all chains $z[n]$ is pre-compensated with the most recent phase estimate

$$\tilde{z}_{m,l}[n] = z[n] \cdot e^{-j\hat{\theta}_{m,l}} \cdot \text{rect}\left[\frac{n - \tau_{\text{TX},l}}{t_{\text{dm}}}\right], \quad (7)$$

where $\hat{\theta}_{m,l}$ is the phase estimate for chain m from the l -th calibration interval $[l-1, l]t_{\text{obs}}$, and $\tau_{\text{TX},l} = t_{\text{syn}} + t_{\text{dm}}/2 + lt_{\text{obs}}$ centers the data block within the transmission window Fig. 2. Note that the rectangular expression is used to apply the phase estimate to the data signal block (blue element in Fig. 2). Then the corresponding quasi-coherent transmitted pass-band signal is

$$\begin{aligned} \tilde{s}_l(t) &= \sum_{m=1}^M \tilde{z}_{m,l}(t) e^{j(2\pi f_{c,m} t + \theta_{\text{OS},m}(t) + \theta_{\text{RF},m})} \\ &= \sum_{m=1}^M z(t) e^{j(2\pi f_{c,m} t + \theta_m(t) - \hat{\theta}_{m,l})} \cdot \text{rect}\left[\frac{t - \tau_{\text{TX},l}}{t_{\text{dm}}}\right], \end{aligned} \quad (8)$$

with $\theta_m(t) = 2\pi\Delta f_m t + \theta_{\text{OS},m}(t) + \theta_{\text{RF},m}$ and $\Delta f_m = f_{c,m} - f_c$.

B. Phase Noise Model

IEEE defines phase noise as the random fluctuation in the phase of a periodic signal, typically characterized in the frequency domain by its spectral density [10]. In the time domain, this fluctuation manifests as timing error, or jitter. The phase error resulting from the timing error at chain m for an oscillator operating at frequency f_c is $\theta_{\text{OS},m}(t) = 2\pi f_c \alpha_m(t)$.

In the case of a free running VCO, the jitter can be

represented by a Wiener process [11]. In continuous time,

$$\alpha_{\text{vco}}(t) = \sqrt{c_{\text{vco}}} \int_0^t \xi(t') dt', \quad (9)$$

where c_{vco} is the oscillator constant and $\xi(t)$ represents a Gaussian process with unit variance. When this process is sampled at T_s to obtain $\xi(iT_s)$ discrete increments, the jitter can be written as

$$\alpha_{\text{vco}}[n] = \begin{cases} 0, & n = 0 \\ \sqrt{c_{\text{vco}}T_s} \sum_{i=0}^{n-1} \xi(iT_s), & n > 0 \end{cases}. \quad (10)$$

Note that to obtain the Wiener process, the Gaussian process is scaled with the oscillator constant c_{vco} . This yields a $1/f^2$ phase noise spectrum with 3 dB bandwidth $f_{3\text{dB}} = \pi f_c^2 c_{\text{vco}}$.

In a PLL, the VCO is placed in a control loop that suppresses long-term drift by comparing its output to a stable reference signal. It is assumed that both reference oscillator and VCO can be modeled as free running oscillators and that the PLL is in locked state. Then the PLL output jitter in discrete time is given by [12]

$$\alpha_{\text{PLL}}[n] = \begin{cases} 0, & n = 0 \\ \sum_{i=0}^{n-1} (\alpha_{\text{PLL}}[i] - \alpha_{\text{REF}}[i]) \\ \cdot (-2\pi f_{\text{PLL}} T_s) + \alpha_{\text{vco}}[n-1], & n > 0 \end{cases}. \quad (11)$$

The bandwidth of the PLL is represented by f_{PLL} and c_{REF} refers to the oscillator constant of the reference oscillator.

The software-defined radio (SDR) platforms used in our measurements employ PLL's locked to a common 10 MHz reference. The model for a PLL can be simplified under the following conditions:

- 1) the oscillator constant for the reference oscillator is sufficiently high so that during an observation period t_{obs} the condition $c_{\text{vco}} \gg c_{\text{REF}}$ applies,
- 2) the PLL bandwidth is sufficiently high $f_{\text{PLL}} \gg f_{3\text{dB}}$,
- 3) the process is sampled so that $\frac{1}{T_s} > f_{\text{PLL}}$,
- 4) the observation time is short $t_{\text{obs}} < \frac{c_{\text{vco}} - 3c_{\text{REF}}}{c_{\text{REF}} 2\pi f_{\text{PLL}}}$ [12].

Then, the jitter at PLL output can be treated as white noise and described by $\alpha_{\text{PLL}}[n] = \alpha_0 + w[n]$, where $w[n] \sim \mathcal{N}(0, c_{\text{vco}}T_s)$ is white Gaussian noise. The term $\alpha_0 \sim \mathcal{U}(0, f_c^{-1})$ refers to a uniformly distributed constant time shift. Compensating this constant offset is essential for initial phase alignment, while periodic calibration tracks the time-varying component $w[n]$. In continuous time the phase of RF chain m is $\theta_m(t) = 2\pi f_c \alpha_{\text{PLL},m}(t)$. This approximation is validated through measurements in the following section.

III. MEASUREMENT RESULTS

A. Measurement Setup

Fig. 3 shows the measurement setup used to evaluate the proposed real-time phase calibration method. The system follows the architecture described in [13]. Each TX RF chain transmits the synchronization signal in a TDMA scheme. The synchronization signal is transmitted over cable to receiver chain RF1 to isolate the phase noise of the transmit chains from channel-induced variations. From this recorded signal,

TABLE I
SYSTEM PARAMETERS MEASUREMENT.

Parameter	Symbol	Value
Carrier frequency	f_c	3.75 GHz
Bandwidth	B	1 MHz
Sample frequency	f_s	4 MHz
TX RF chains	M	6
Observations	L	10000
Obs. Interv.	t_{obs}	100 ms
Samples	N	2500

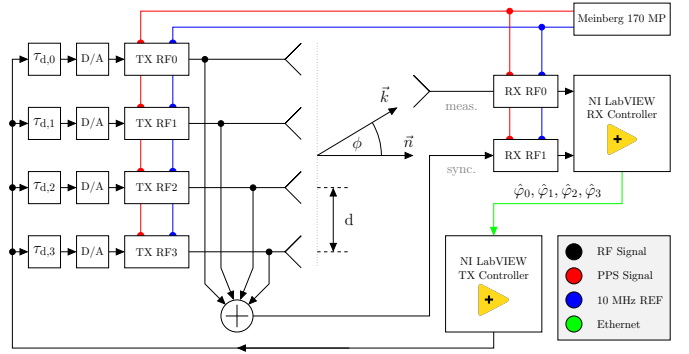


Fig. 3. System setup for transceiver with 4 TX and real-time calibration [13].

the RX controller estimates the phases of the transmitting RF chains. These phase estimates are sent to the TX controller on a host PC for precoding to allow for coherent transmission as shown in eq. (7).

Measurements were performed on six transmit chains using three different versions of the universal software radio peripheral (USRP) X310. Key parameters for the measurement are given in Table I. With observation interval $t_{\text{obs}} = 100$ ms and $L = 10000$ observations, the total measurement duration was

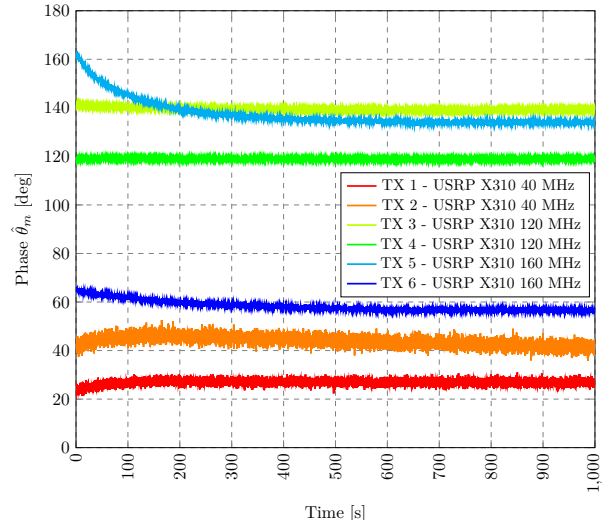


Fig. 4. Estimated phases for 6 transmit chains [14].

1000 s. Fig. 4 illustrates the estimated phases over time.

Several observations can be made from the measurement data [14] shown in Fig. 4. During the first 250 s of operation, the phases of TX5 and TX6 (cyan and blue traces) drift by approximately 25° and 5° , respectively, despite all chains sharing a common 10 MHz reference. This effect is likely caused by temperature-induced changes in the phase response of the RF frontend during warm up. Other chains such as TX3 and TX4 (lime and green trace) and exhibit negligible drift during the measurement. This is likely due to these chains being already warm from previous measurements when the recording began. These observations highlight the importance of allowing sufficient warm up time of RF components in practical deployments. As demonstrated in the following subsections, the proposed calibration method is suitable for tracking these phase variations, enabling coherent transmission despite this temperature induced drift.

B. Jitter distribution

Analyzing the PDF of the timing jitter provides insight into the effectiveness of the proposed calibration methods. The jitter for chain m at observation interval l is obtained from the phase estimates as

$$\alpha_{m,l} = \frac{\hat{\theta}_{m,l}}{2\pi f_c}. \quad (12)$$

The PDF is estimated using a Gaussian kernel density estimate (KDE) applied to the measured jitter values.

Two calibration approaches are considered:

- **Instantaneous calibration:** precoding with most recent phase estimate as in Eq. (7)
- **Smoothed calibration:** precoding using the average of the last 10 phase estimates, $\frac{1}{10} \sum_{k=0}^9 \hat{\theta}_{m,l-k}$, to reduce estimation noise.

As a quantitative metric, the root mean square (RMS) cycle-to-cycle jitter is used with definition

$$\tau_{\text{RMS},m} = \frac{1}{2\pi f_c} \sqrt{\frac{1}{L-1} \sum_{l=0}^{L-1} |\hat{\theta}_{m,l+1} - \hat{\theta}_{m,l}|^2}. \quad (13)$$

Note that this metric is valid only when the phase is sufficiently stationary over the observation period [15].

Fig. 5, 6, and 7 show the jitter PDF's for TX1, TX4 and TX5, illustrating different time-dependent phase responses. Table II summarizes the corresponding RMS jitter values.

1) **RF Chains with Negligible Drift:** TX1 Fig. 5 exhibits negligible drift during the total measurement duration, with a near-Gaussian jitter distribution (red) and RMS value of 1.66 ps. Instantaneous calibration (orange) slightly increases the RMS jitter to 2.06 ps. This effect occurs because the calibration correction applied in eq. (9) effectively differentiates the phase, which amplifies high-frequency noise. The increase is small relative to the uncalibrated jitter, indicating that calibration is not necessary when drift is negligible. Smoothed calibration (lime) reduces the jitter to 1.39 ps.

TABLE II
RMS CYCLE-TO-CYCLE JITTER FOR DIFFERENT TX.

	No calib.	Inst. calib.	Sm. calib.
TX1	1.66 ps	2.06 ps	1.39 ps
TX2	3.03 ps	3.20 ps	2.15 ps
TX3	728 fs	199 fs	134 fs
TX4	193 fs	183 fs	124 fs
TX5	7.78 ps	891 fs	632 fs
TX6	2.99 ps	893 fs	630 fs

TX4 Fig. 6 shows low intrinsic jitter (193 fs RMS). Instantaneous calibration yields marginal improvement (183 fs RMS), while smoothed calibration achieves 124 fs RMS.

2) **RF Chains with Significant Drift:** TX5 Fig. 7 exhibits significant drift, as evident from its PDF without calibration (cyan, 7.78 ps RMS). Instantaneous calibration effectively compensates this drift, resulting in a Gaussian distribution (blue, 891 fs RMS). Smoothed calibration further reduces jitter to 632 fs RMS (violet), demonstrating the benefit of averaging.

After calibration, the RMS jitter is consistent within each USRP variant: TX3 and TX4 (124 to 134 fs) and TX5 and TX6 (630 to 632 fs) show excellent agreement. TX1 and TX2 (1.39 to 2.15 ps) exhibit more variation but remain within the same order of magnitude.

C. Quantile-Quantile Plot

A quantile-quantile (Q-Q) plot is a graphical method for comparing the similarity of a distribution to the normal distribution. In this plot, the quantiles of the evaluated distribution (typically on the y-axis) are plotted against the quantiles of a normal distribution (typically on the x-axis). The distributions are normalized by their standard deviations to allow for even comparison. If a distribution function matches the normal distribution, the Q-Q plot data points fall on a straight line (see Fig. 8 black trace).

Fig. 8 shows the Q-Q plot for the estimated phases before calibration. The distributions for TX3, TX5, and TX6 deviate substantially from the reference line, indicating a non-Gaussian PDF. This is consistent with Fig. 4, which shows significant drift for TX5 and TX6 over the measurement duration. From Fig. 7 it can also be seen that the PDF for TX5 (cyan) is not Gaussian and that the phase of this chain drifts during the measurement. For the other RF chains TX1, TX2 and TX4 the distributions are approximately Gaussian. In contrast, TX1, TX2, and TX4 are approximately Gaussian, though TX1 exhibits slight deviation at the tails of its distribution at higher quantiles.

After applying the proposed calibration, the Q-Q plot in Fig. 9 shows that all distributions align closely with the normal distribution. This indicates that the residual jitter and corresponding phase errors are Gaussian distributed, which suggests that the calibration has effectively whitened the phase noise. A slight deviation at the tails of the distribution (± 2 standard deviations) is still visible. However, this affects only

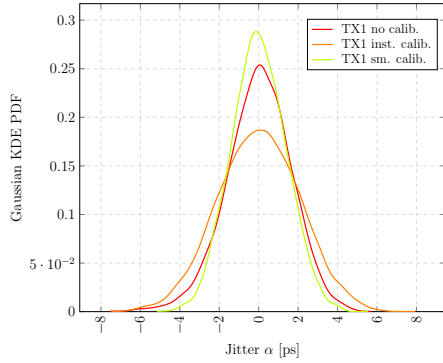


Fig. 5. PDF for TX1 before/after calibration

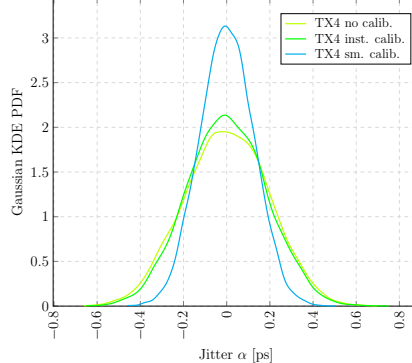


Fig. 6. PDF for TX4 before/after calibration

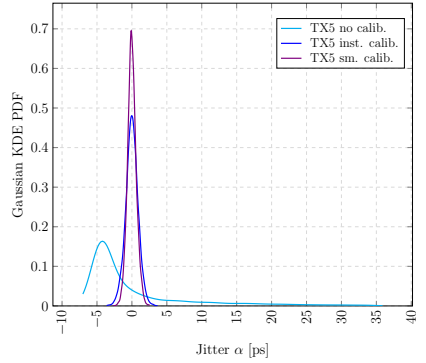


Fig. 7. PDF for TX5 before/after calibration

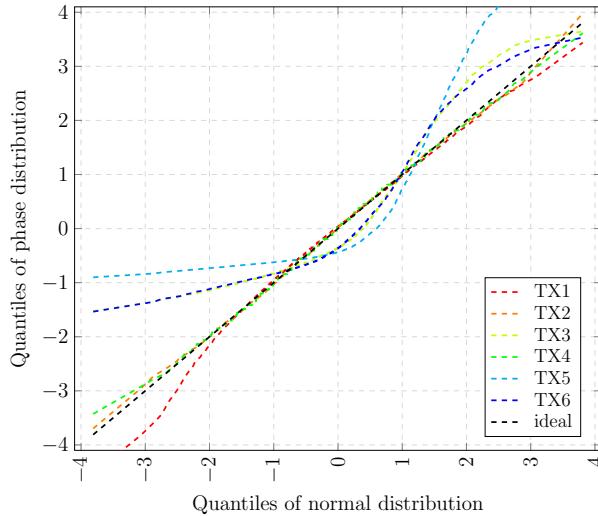


Fig. 8. Measured quantiles of phase plotted over quantiles of normal distribution

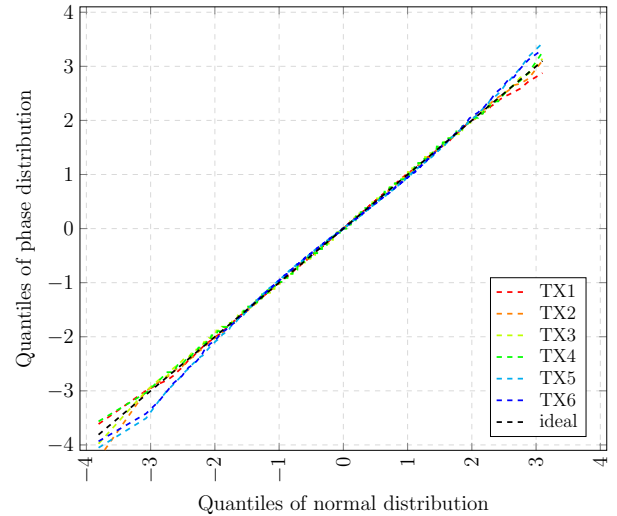


Fig. 9. Quantiles of phase after calibration plotted over quantiles of normal distribution

a small fraction of the distribution. Within the central 95% of the probability mass, the fit to a normal distribution is decent.

IV. SIMULATION RESULTS

Numerical simulations are performed to complement the hardware measurements by allowing systematic variation of the observation interval t_{obs} , enabling investigation of calibration performance beyond the fixed conditions of the experimental setup.

A. Effect of Calibration in Time Domain

When continuous calibration is applied, the observation interval t_{obs} has a direct effect on the residual jitter. This section investigates this relationship for both free-running VCO and a PLL, with RMS of the cycle-to-cycle jitter τ_{RMS} as defined in eq. (13) as a metric. Key simulation parameters are listed in Table III.

Fig. 10 shows the RMS of the jitter processes for the uncalibrated and calibrated case, at different observation intervals. Two theoretical lower bounds are also shown: $\sqrt{c_{\text{VCOT}} t_{\text{obs}}}$

for the VCO and $\sqrt{c_{\text{REF}} t_{\text{obs}}}$ for the PLL, representing the fundamental limits set by oscillator properties.

1) *Free-Running VCO*: For the uncalibrated VCO (black trace), τ_{RMS} increases with t_{obs} , consistent with the variance scaling $\sigma^2 = c_{\text{VCOT}}$ [12]. Both instantaneous and smoothed calibration (lime and violet traces) achieve the theoretical lower bound $\sqrt{c_{\text{VCOT}} t_{\text{obs}}}$ across all observation intervals, confirming that the calibration method optimally compensates the VCO phase noise.

2) *Phase-Locked-Loop*: The uncalibrated PLL (blue trace) exhibits a similar behaviour, with a increase of τ_{RMS} over t_{obs} . After calibration, three observations stand out. First, smoothed calibration consistently outperforms the instantaneous calibration by a slight margin. Second, the calibrated jitter RMS for longer intervals is asymptotically bounded by the reference oscillator limit $\sqrt{c_{\text{REF}} t_{\text{obs}}}$ (orange trace). Third, below approximately 10 ms, the jitter reaches a floor and does not improve with shorter t_{obs} . This however is not due to a limitation on the calibration but innate properties of a PLL. In the transition region between VCO-dominated and

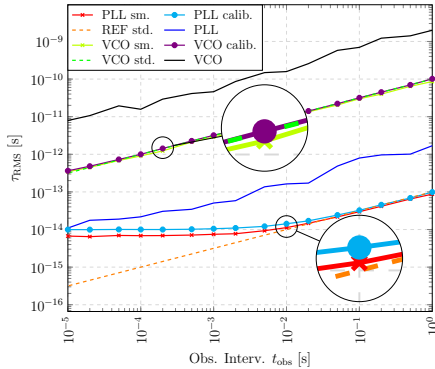


Fig. 10. RMS of Cycle-to-cycle jitter for different observation intervals.

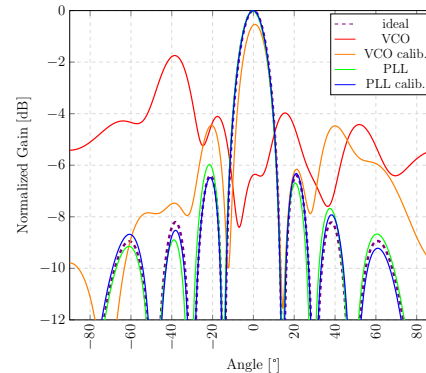


Fig. 11. Array response under phase impairments with and without periodic calibration

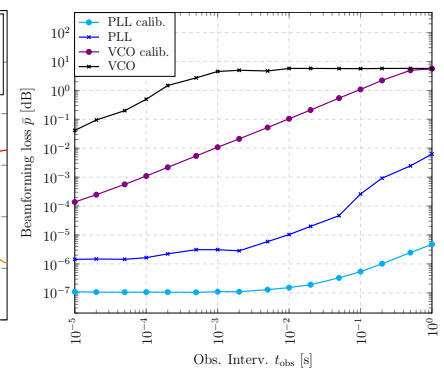


Fig. 12. Average beamforming loss in steering direction for different observation intervals

reference oscillator-dominated regimes, the PLL jitter variance is bounded by [12]

$$\sigma^2 = \frac{c_{\text{VCO}} - 3c_{\text{REF}}}{4\pi f_{\text{PLL}}}. \quad (14)$$

For the given parameters in Table III this evaluates to a variance of $7.957 \times 10^{-28} \text{ s}^2$, with RMS jitter of $2.821 \times 10^{-14} \text{ s}$. The smoothed calibration trace in Fig. 10 reaches exactly this value, demonstrating that the proposed method achieves the fundamental performance bound for PLL's.

B. Effect of Calibration on Beamforming

On the transmit side, coherence of the RF chains in a fully digital array is essential to allow for beamforming. Consequently, significant imperfections in phase calibration of the array will result in a loss in beamforming gain in the desired steering direction.

Fig. 11 shows the array response at boresight for arrays affected by VCO and PLL phase impairments, assuming an initial calibration has been performed, with and without subsequent periodic calibration. Without periodic calibration, the array subjected to phase noise from a VCO (red trace) shows no coherent beamforming pattern. With periodic calibration (orange trace), a clear main lobe emerges. A small offset from the ideal gain remains, as the VCO jitter over the 100 ms observation interval is still significant.

Since the PLL output process does not drift significantly for the considered observation interval, the array response even without applying periodic calibration (green trace) is already near ideal. Applying the calibration procedure to compensate the PLL jitter process (blue trace) yields only a small improvement in the side lobes. For the PLL the cases with and without periodic calibration achieve near-optimal beamforming gain. This is because the PLL holds its output phase nearly constant over the 100 ms observation interval, exhibiting negligible drift.

As a metric to assess the beamforming performance with and without periodic calibration, the average beamforming loss in steering direction is considered. This average beamforming loss \bar{p} is calculated as the difference between ideal gain and

TABLE III
SYSTEM PARAMETERS SIMULATION.

Parameter	Symbol	Value
Carrier frequency	f_c	3.75 GHz
Sample frequency	f_s	20 MHz
TX RF chains	M	8
Observations	L	1000
Obs. Interv.	t_{obs}	$\{1 \text{ ms}, \dots, 10 \mu\text{s}\}$
Samples	N	100
Osc. Const. VCO	c_{VCO}	$1 \times 10^{-20} \text{ s}$
Osc. Const. REF	c_{REF}	$1 \times 10^{-26} \text{ s}$
PLL Bandw.	f_{PLL}	1 MHz

obtained gain in steering direction and averaged over steering angles $\phi \sim \mathcal{U}(-60^\circ, 60^\circ)$.

Fig. 12 shows the average beamforming loss for VCO and PLL cases with and without periodic calibration. For the considered array size, a maximum gain of 6 dB can be achieved. This value corresponds to the loss observed for the VCO without periodic calibration (black trace) at longer observation intervals. Below an observation interval of $\approx 1 \text{ ms}$, the loss declines. This is due to the observation interval being sufficiently short that the VCO cannot drift that far in this time period, allowing the initial calibration to remain partially effective. When the VCO jitter is periodically calibrated for (violet trace) but the observation interval is long (1 s), there is no improvement over the case with only initial calibration. This is due to the VCO drifting sufficiently far between calibration times, rendering beamforming ineffective. For all shorter observation intervals, periodic calibration yields a significant improvement in beamforming loss.

In the case of a PLL with only initial calibration (blue trace), the beamforming loss is negligibly small meaning that there is no need for periodic calibration with the given choice of parameters. Still, periodic calibration (cyan trace) can further reduce this loss by approximately an order of magnitude. For short observation intervals below 1 ms the beamforming loss reaches a floor. This corresponds to the fundamental PLL jitter limit as discussed previously and observed also in Fig. 10.

V. CONCLUSION

Commonly known methods for compensation of phase noise in MIMO systems typically apply phase noise calibration at the receiver. However, transmit-side beamforming with large arrays requires real-time phase coherence across all RF chains during transmission. This paper has presented and validated a simple method for real-time phase calibration of fully digital transmit arrays.

Two calibration approaches were compared: instantaneous compensation using the most recent phase estimate, and smoothed compensation using a time average of the last 10 estimates. Measurements on six USRP X310 chains demonstrated that both methods significantly reduce phase drift and jitter. Key results include:

- RMS cycle-to-cycle jitter reduced to as low as 124 fs for PLL's, with smoothed calibration consistently outperforming instantaneous calibration.
- Thermal drift of up to 25° observed during warm-up period, despite a common 10 MHz reference, highlighting the need for calibration even with shared reference oscillator.
- After calibration, residual phase errors are Gaussian distributed, as confirmed by QQ plot analysis, indicating whitening of the phase noise.
- Simulation results showed that the proposed method achieves the fundamental PLL jitter limit of 2.28×10^{-14} s for the given system parameters and optimal choice of observation interval duration.

These results demonstrate that the proposed low-complexity calibration methods are well-suited for synchronizing SDR-based testbeds and ensuring coherence in MIMO channel measurements.

Future work could extend this approach to joint transmitter-receiver calibration, integrate it with over-the-air reciprocity calibration methods, and investigate its performance under mobile conditions where Doppler effects become significant.

ACKNOWLEDGMENT

This work was supported by BMBF under the project KOMSENS-6G (16KISK124).

REFERENCES

- [1] A. Pitarokilis, S. K. Mohammed, and E. G. Larsson, "Uplink performance of time-reversal mrc in massive mimo systems subject to phase noise," *IEEE Transactions on Wireless Communications*, vol. 14, no. 2, pp. 711–723, 2015.
- [2] F. Liu, Y. Cui, C. Masouros, J. Xu, T. X. Han, Y. C. Eldar, and S. Buzzi, "Integrated sensing and communications: Toward dual-functional wireless networks for 6g and beyond," *IEEE Journal on Selected Areas in Communications*, vol. 40, no. 6, pp. 1728–1767, 2022.
- [3] E. 3GPP, "5G NR; Physical channels and modulation," Technical Specification (TS) 38.211, 01 2026, v19.2.0.
- [4] S. Prager, M. S. Haynes, and M. Moghaddam, "Wireless subnanosecond rf synchronization for distributed ultrawideband software-defined radar networks," *IEEE Transactions on Microwave Theory and Techniques*, vol. 68, no. 11, pp. 4787–4804, 2020.
- [5] J. Querol, J. C. Merlano-Duncan, L. Martinez-Marrero, J. Krivochiza, S. Kumar, N. Maturo, A. Camps, S. Chatzinotas, and B. Ottersten, "A cubesat-ready phase synchronization digital payload for coherent distributed remote sensing missions," in *2021 IEEE International Geoscience and Remote Sensing Symposium IGARSS*, 2021, pp. 7888–7891.
- [6] M. Jokinen, O. Kursu, N. Tervo, A. Paerssinen, and M. E. Leinonen, "Over-the-air phase calibration methods for 5g mmw antenna array transceivers," *IEEE Access*, vol. 12, pp. 28 057–28 070, 2024.
- [7] Y. Cao, P. Wang, K. Zheng, X. Liang, D. Liu, M. Lou, J. Jin, Q. Wang, D. Wang, Y. Huang, X. You, and J. Wang, "Experimental performance evaluation of cell-free massive mimo systems using cots rru with ota reciprocity calibration and phase synchronization," *IEEE Journal on Selected Areas in Communications*, vol. 41, no. 6, pp. 1620–1634, 2023.
- [8] C. Studer, M. Wenk, and A. Burg, "Mimo transmission with residual transmit-rf impairments," in *2010 International ITG Workshop on Smart Antennas (WSA)*, 2010, pp. 189–196.
- [9] S. M. Kay, *Fundamentals of statistical signal processing: estimation theory*. USA: Prentice-Hall, Inc., 1993.
- [10] IEEE, "Ieee standard for jitter and phase noise," *IEEE Std 2414-2020*, pp. 1–42, 2021.
- [11] A. Demir, A. Mehrotra, and J. Roychowdhury, "Phase noise in oscillators: a unifying theory and numerical methods for characterization," *IEEE Transactions on Circuits and Systems I: Fundamental Theory and Applications*, vol. 47, no. 5, pp. 655–674, 2000.
- [12] C. Collmann, B. Banerjee, A. Nimr, and G. Fettweis, "A practical analysis: Understanding phase noise modelling in time and frequency domain for phase-locked loops," 2025. [Online]. Available: <https://arxiv.org/abs/2507.12146>
- [13] C. Collmann, A. Nimr, and G. Fettweis, "Reliable angle estimation in true-time-delay systems with real-time phase calibration," in *2025 IEEE 5th International Symposium on Joint Communications & Sensing (JC&S)*, Oulu, Finland, Jan 2025, p. 2.
- [14] C. Collmann, "Phase measurements for coherent transmission in mimo system with usrp x310," 2026. [Online]. Available: <https://dx.doi.org/10.21227/vnn4-cz93>
- [15] M. Loehning, "Analyse und modellierung der effekte von abtast-jitter in analog-digital-wandlern," Doctoral Dissertation, TU Dresden, Dresden, 2006.